RSC Advances

PAPER

View Article Online
View Journal | View Issue

Cite this: *RSC Adv.*, 2023, **13**, 1751

Microwave-assisted synthesis of octahedral Rh nanocrystals and their performance for electrocatalytic oxidation of formic acid †

Xiaomeng Liu, Junxuan Xu, Haoyue Zhang, Yitian Zhong, Haosheng Feng, Yanxi Zhao, Qin Li, Xianghong Li and Tao Huang *

Received 23rd November 2022
Accepted 27th December 2022

DOI: 10.1039/d2ra07445a

rsc.li/rsc-advances

Uniform and well-defined octahedral Rh nanocrystals were rapidly synthesized in a domestic microwave oven for only 140 s of irradiation by reducing $Rh(acac)_3$ with tetraethylene glycol (TEG) as both a solvent and a reducing agent in the presence of an appropriate amount of KI, didecyl dimethyl ammonium chloride (DDAC), ethylene diamine (EDA) and polyvinylpyrrolidone (PVP). KI, DDAC and EDA were essential for the creation of octahedral Rh nanocrystals. Electrochemical measurements showed a significantly enhanced electrocatalytic activity and stability for the as-prepared octahedral Rh nanocrystals compared with commercial Rh black.

To date, platinum group metals play an indispensable role as efficient catalysts for some important reactions in industry. However, due to their limited reserves and high prices, a large number of platinum group metal nanoparticles with different particle sizes, morphologies and surface structures have been synthesized by means of various methods to reduce their cost.[1] As a platinum group metal, Rh has good catalytic activity and stability, and is often used as a typical catalyst for some chemical reactions such as hydrogenation,[2–7] nitrogen oxide reduction,[8] CO oxidation,[9–11] cross coupling,[12–14] hydroformylation,[15–19] in fuel cells[20,21] and other chemical reactions.[22] Therefore, controlled syntheses of Rh nanoparticles with different morphologies have attracted much attention. In recent years, people have successfully prepared Rh nanostructures with various morphologies such as sheet,[23–27] flower,[6] polyhedron,[28–33] porous ball,[8] multi branches,[34–39] stars,[40] nanoframes[13,14,41] and nano nail.[42] These Rh nanoparticles with unique structures effectively improve the atom utilization as well as their catalytic reaction performances. However, similar to other platinum group metals, the difficulty of large-scale preparation of Rh nanomaterials with single morphology and uniform size still greatly restricts their industrial application.

Microwave irradiation has been widely used in chemical synthesis because of its simple, rapid and efficient characteristics as well as special heating mode from the inner. We have synthesized many metallic nanoparticles with different shapes by using microwave irradiation for about 80 to 120 seconds. Herein, we report a simple and fast strategy for the synthesis of octahedral Rh nanocrystals under microwave irradiation with using domestic microwave oven. In a typical synthesis, octahedral Rh nanocrystals with uniform and well-defined morphologies were successfully synthesized with $Rh(acac)_3$ as the precursor, polyvinyl pyrrolidone (PVP) as the stabilizer, triethylene glycol (TEG) as both a solvent and a reducing agent in the presence of didecyl dimethyl ammonium chloride (DDAC), KI and ethylene diamine (EDA) under microwave irradiation in a very short time. Meanwhile, the electrocatalytical performance of the as-prepared octahedral Rh nanocrystals for the electrooxidation of formic acid was also investigated with commercial Rh black as a contrast.

The TEM and SEM images of the representative Rh nanoparticles obtained under the optimal experimental conditions are shown in Fig. 1, S1 and S2.† Wherein, the prepared Rh nanoparticles demonstrated uniform and well-defined octahedral structure with sharp edges and corners as well as smooth surfaces (Fig. 1a and b), in which the average side length is about 65 nm. The high-resolution TEM (HRTEM) image (Fig. 1c) shows well-resolved continuous fringes clearly. The corresponding fast Fourier transform (FFT) pattern, as the inset shown in Fig. 1c, shows a lattice distance of 0.194 or 0.216 nm, which can be attributed to the {200} and {111} lattice planes of the octahedral Rh with face-centered cubic structure, respectively, confirming its single-crystal nature. Furthermore, the regular octahedral feature of the as-prepared Rh nanoparticles can be well distinguished from SEM images, as shown in Fig. 1d and S2.† These results show that the octahedral Rh nanocrystals with a single morphology can be rapidly synthesized in a great

Key Laboratory of Catalysis and Energy Materials Chemistry of Ministry of Education, College of Chemistry and Materials Science, South-central Minzu University, Wuhan 430074, China. E-mail: huangt208@163.com

† Electronic supplementary information (ESI) available: Experimental details, TEM, SEM images and cyclic voltamograms. See DOI: https://doi.org/10.1039/d2ra07445a

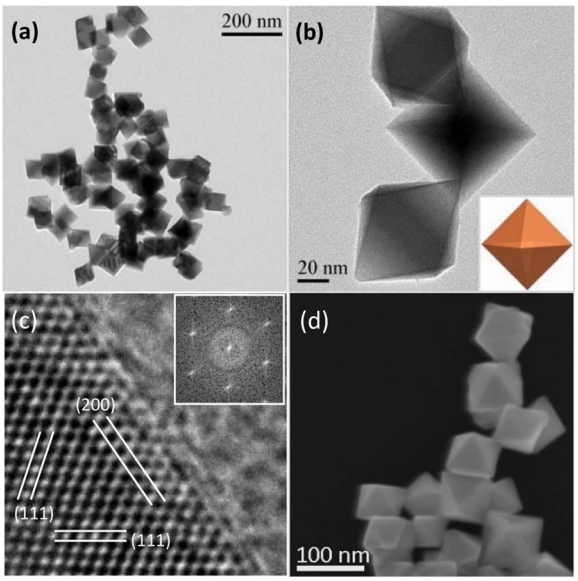

Fig. 1 TEM and SEM images of the as-prepared octahedral Rh nanocrystals. (a) and (b) Typical TEM images with different scales. The inset in (b) is the schematic illustration; (c) typical HRTEM image. The inset is the corresponding FFT pattern; (d) SEM image.

quantity by irradiation with domestic microwave oven for only 140 s.

Fig. 2a shows the XRD pattern of the as-prepared typical octahedral Rh nanocrystals. As can be seen, the diffraction peaks at 2θ values of 41.26, 47.95, 70.18 and 84.33° are observed, which can be well indexed to the diffractions of (111), (200), (220) and (311) lattice facets of metallic Rh referring to the standard powder diffraction card (JCPDS card No. 05-0685), respectively. This observation further confirmed their *fcc* Rh structure. In addition, the narrow and sharp (111) diffraction peak implied that the typical octahedral Rh nanocrystals exhibited a high purity and crystallinity. The XPS spectrum was taken for the as-prepared octahedral Rh nanocrystals and the result was displayed in Fig. 2b, As it can be seen, two peaks corresponding to the electron binding energies of Rh $3d_{3/2}$ and Rh $3d_{5/2}$ were observed at 311.85 eV and 307.10 eV with an interval of 4.75 eV, respectively, which were consistent with the literature values (311.75 and 307.0 eV),[43] revealing Rh(0) metallic state of the octahedral nanocrystals.

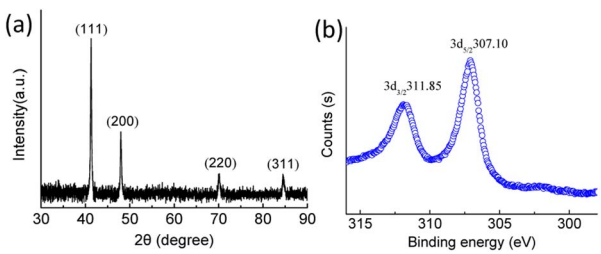

Fig. 2 XRD pattern (a) and XPS spectrogram (b) of octahedral Rh nanocrystals.

The dependence of the morphological evolution of Rh nanocrystals upon irradiation time was investigated. When irradiated for 120 s, the octahedral structural Rh nanocrystals with about 65 nm of the side length produced except for unclear edges and corners as well as a shorter side length, as shown in Fig. 3a. As microwave irradiation progressed to 140 s, uniform and well-defined octahedral Rh nanocrystals with smooth surfaces generated (Fig. 3b). While the irradiation time was extended to 160 s, however, the vertices of some octahedral structures were truncated although with no change of the sizes, as shown in Fig. 3c. As the irradiation time reached 180 s, the octahedral structural feature of most particles disappeared with a further truncation of their vertices (Fig. 3d), which should be ascribed to higher surface free energies for the metallic atoms at the apexes and edges as well as a higher internal temperature due to a longer irradiation time. These results indicated that the optimum microwave irradiation time was 140 s for the creation of regular octahedral Rh nanocrystals.

It was noteworthy that KI played a crucial role in controlling synthesis of octahedral Rh nanocrystals. When no KI was used, it would produce irregular Rh nanoparticles, as shown in Fig. 4a. While with addition of 0.6 mmol of KI, octahedral Rh nanostructures with blunt vertices and an average side length of about 50 nm were generated (Fig. 4b), implying an incomplete growth relative to the case of 0.8 mmol of KI as in the typical experimental process (Fig. 1). Nevertheless, the amount of KI was increased to 1.2 mmol, only less octahedral structure features could be observed except for few obscure polyhedral outlines (Fig. 4c). These results indicated that the existence of KI was advantageous to the generation of octahedral Rh nanocrystals. Generally, the eight triangular surfaces of metallic Rh octahedron consists of (111) lattice planes. According to the previous report,[44–49] it can be considered that the preferential adsorption of I^- anions on Rh (111) planes is one of the main

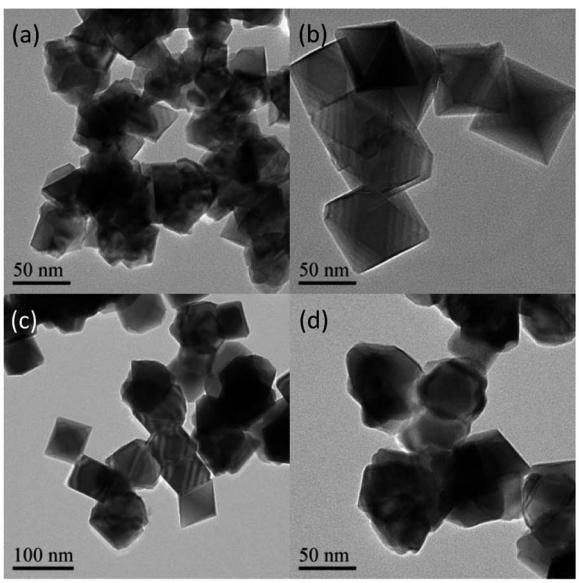

Fig. 3 TEM images of Rh nanoparticles prepared at different reaction time. (a) 120 s; (b) 140 s; (c) 160 s; (d) 180 s.

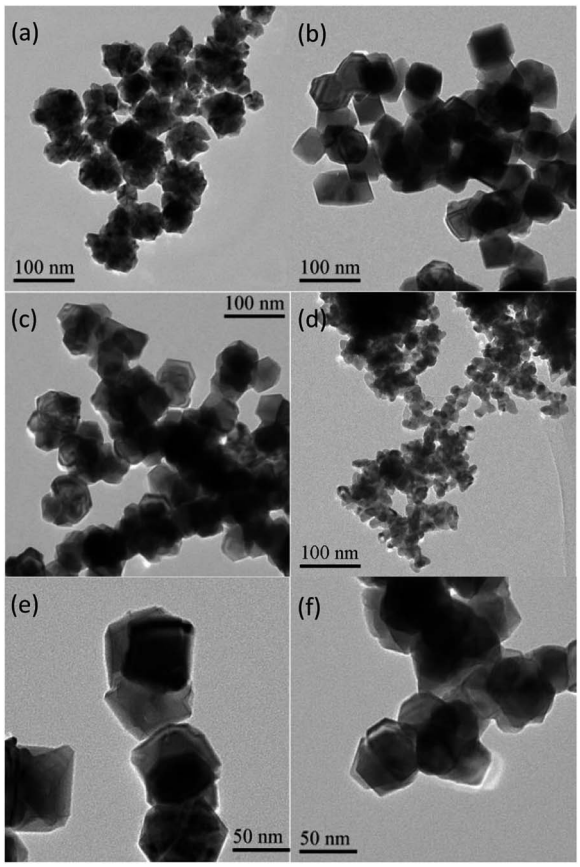

Fig. 4 TEM images of Rh nanoparticles prepared with different amounts of DDAC or KI under the same other conditions. (a) Absence of KI; (b) 0.6 mmol of KI; (c) 1.2 mmol of KI; (d) absence of DDAC; (e) 0.2 mmol of DDAC; (f) 0.6 mmol of DDAC.

factors driving the formation of octahedral structure. As a result, a growth along ⟨111⟩ directions was confined and a growth along ⟨100⟩ directions was facilitated, which created octahedral structures due to anisotropic growth. However, excessive I^- ions would adsorb non-selectively on the surfaces of Rh nanoparticles, which resulted in passivation of the edges and corners of polyhedron. In addition, an equivalent amount of KBr or KCl was used instead of KI, respectively, to clarify the role of I^- ions under the same other conditions. As can be seen (Fig. S3, ESI†), no octahedral Rh nanocrystal except for agglomerated irregular nanosheets was observed in these two contrast experiments. This may be ascribed to the change of the precursor. In the presence of a large number of I^- ions, the precursor can be transformed to a more stable $[RhI_6]^{3-}$ complex.[44–47] As a result, the reducing rate of Rh(III) to Rh atom decreased, which may be favourable for the nucleation of Rh nanoparticles and the oriented growth of Rh octahedra.

Meanwhile, the influence of DDAC on the generation of octahedral Rh nanocrystals was also studied under the same other conditions. In the absence of DDAC, only agglomerated irregular Rh nanoparticles were observed (Fig. 4d). When 0.2 mmol of DDAC was added, octahedral Rh nanostructures with an average side length of about 45 nm, a smaller size relative to the case of 0.4 mmol of DDAC as in the typical experiments (Fig. 1), were generated accompanying with a few irregular nanoparticles (Fig. 4e). With increasing the amount of DDAC to 0.6 mmol, agglomerated irregular polyhedral nanostructures formed (Fig. 4f). Thus, the addition of DDAC was also indispensable for the growth of octahedral Rh nanostructures under microwave irradiation. Whereas an excessive amount of DDAC was also unfavourable for creation of the octahedral Rh nanocrystals. Moreover, no octahedral nanostructures generated except for urchin-like Rh hierarchical superstructures when adding an equivalent amount of cetyltrimethylammonium chloride (CTAC) instead of DDAC (Fig. S4a, ESI†). While didoctyl dimethyl ammonium bromide (DDAB) was used instead of DDAC, the formation of octahedral Rh structures can be still observed although accompanying with other irregular polyhedral (Fig. S4b, ESI†). These results suggested that the formation of octahedral Rh nanostructures were strongly dependent upon the hydrophobic chains of DDAC or DDAB but nothing to do with Cl^- or Br^- anions. The effect of other halide ions can be ignored due to the existence of a large number of I^- ions. That is because the strength of adsorption of I^- ions on metal surfaces is generally stronger than that of Cl^- or Br^- ions.[48]

Accordingly, the generation of octahedral Rh nanocrystals should be ascribed to the synergistic effect of KI and DDAC under the above experimental conditions. We believe that DDAC could enhance the role of I^- ions in generating (111) facets of octahedral by adjusting the adsorption selectivity of I^- ions on (111), (100) or (110) facets. On the one hand, the amount of KI would manipulate the reducing kinetics to form octahedral Rh nanostructures under microwave irradiation. A slow reducing rate was favourable for the oriented growth of Rh octahedra due to the formation of a more stable coordinated anion $[RhI_6]^{3-}$. On the other hand, the confinement of DDAC induced the selective adsorption of I^- ions on Rh {111} facets which restrained the growth along ⟨111⟩ directions of Rh nuclei and prompted the growth along ⟨100⟩ directions. In addition, a proper quantity of DDAC confined the deposition of Rh atoms on {111} facets, which may be beneficial to the growth along ⟨100⟩ directions. However, an excessive amount of DDAC was unfavourable for the formation of shaped Rh nanoparticles since they disturbed the adsorption of I^- anions on Rh {111} facets.

Furthermore, it was also found that ethylene diamine (EDA) demonstrated an important effect on the creation of octahedral Rh nanostructures. Under keeping the total volume of the reaction system unchanged, the significantly agglomerated irregular polyhedral nanoparticles with sharp horns were observed in absence of EDA (Fig. S5a†). When 0.5 mL of EDA was added, a few octahedral nanostructures began to generate though accompanying with agglomerated irregular polyhedra (Fig. S5b†). While the amount of EDA was increased to 1 mL, uniform and well-defined octahedral Rh nanocrystals with flat and smooth surfaces were produced (Fig. S5c†). However, a more amount of EDA was added, a part of octahedral nanostructures become deformation as well as agglomeration (Fig. S5d†). In the reaction system, TEG as a solvent was also

served as a reducing agent. As can be seen, even though without adding EDA, the rhodium salt was still reduced completely to produce metal Rh nanoparticles. With the addition of EDA, octahedral Rh nanocrystals began to generate, while an excessive amount of EDA resulted in unclear edges and corners of the octahedral structures. Obviously, EDA demonstrated significant effect on the morphology control of octahedral Rh nanocrystals. It should be ascribed to the coordination adsorption of EDA on the surface of metal particles.[50] Furthermore, no octahedral nanostructures but irregular nanoparticles or Rh dendrites generated with using an equivalent amount of *n*-butylamine or *n*-octylamine instead of EDA (Fig. S6a and b†). Therefore, we suggest that EDA plays a synergistic role together with DDAC in regulating the rate of atomic packing and nanoparticle growth by coordination adsorption. The growth rate of nanoparticles is faster in absence of EDA, while the growth rate slows down with the increase of EDA dosage. An appropriate amount of EDA facilitates the generation of uniform octahedral Rh nanocrystals by adjusting the balance between nucleation rate and growth rate. Nevertheless, excessive EDA makes a slower growth than nucleation due to their extreme adsorption, resulting in obscure appearances of some octahedral Rh nanoparticles.

In addition, PVP was also found to be important but not essential for the formation of octahedral Rh nanocrystals. Either without or with a few amount of PVP, octahedral Rh nanocrystals can also produce except for a little agglomeration (Fig. S7a and b†). An appropriate amount of PVP contributed to uniform and well dispersed octahedral Rh nanocrystals, while excessive PVP caused aggregation (Fig. S7c and d†). These results indicated that PVP served mainly as a protecting and dispersing agent for the nanocrystals.

The catalytic performance of the synthesized octahedral Rh nanocrystals was tested by cyclic voltammetry (CV) and chronoamperometry (CA) with the formic acid electrooxidation reaction as the model reaction system. Fig. 5a exhibits the representative CV curves obtained for the electrochemical oxidation of 0.5 mol L^{-1} HCOOH over the octahedral Rh nanocrystals and commercial Rh black in 0.5 mol L^{-1} $HClO_4$ solution, respectively. CV measurements showed the peak current density for the octahedral Rh nanocrystals was 3.53 mA cm^{-2} at 0.544 V, while it was 1.01 mA cm^{-2} at 0.609 V for Rh black. The formic acid electrooxidation indicated that the electrocatalytic activity of octahedral Rh nanocrystals was about 3.5 times that of Rh black, demonstrating an obvious morphological dependence for their electrochemical property. The corresponding CA curves of formic acid electro-oxidation at 0.55 V is shown in Fig. 5b. As can be seen, a higher current retention through the whole measuring range were observed over the as-prepared octahedral Rh nanocrystals than Rh black though both of them showed an equivalent attenuation rate in the initial 20 seconds. The CV curve of continuous cycle scanning for octahedral Rh nanocrystals in 0.5 mol L^{-1} $HClO_4$ solution showed a decrease of the electrochemical activity only by 9.6% after 2000 cycles (Fig. S8†). These results reveal that octahedral Rh nanocrystals exhibit a remarkably enhanced electrochemical activity and stability compared with Rh black. Their enhanced catalytic activity should be attributed to the uniform geometric structure with single surface lattice.

Additionally, CO stripping voltammetry measurements were performed. As shown in Fig. S9a,† no CO electro-oxidation (CO_{ox}) was observed for the freshly-prepared octahedral Rh nanocrystals in 0.5 M $HClO_4$ solution. Subsequently, a current peak for CO_{ox} appeared at 0.550 V (*versus* SCE) after adorbing CO for the clean octahedral Rh-modified electrode, as shown in Fig. S9b.† Then CO_{ox} peak disappeared in the following second potential scanning, as shown in Fig. S9c.† These results showed that CO adsorbed on Rh surfaces can be easily removed in the process of electrocatalytic oxidation, showing well CO resistence.

In summary, uniform octahedral Rh nanocrystals could be rapidly prepared with domestic microwave oven in only 140 s of irradiation by reducing $Rh(acac)_3$ with TEG as both a solvent and a reducing agent, PVP as a protecting and dispersing agent in the presence of proper quantities of DDAC, KI and EDA. The formation of octahedral Rh nanocrystals was attributed to the synergism of KI, DDAC and EDA. The electrochemical oxidation of formic acid demonstrated higher electrocatalytic activity and stability for the as-prepared octahedral Rh nanocrystals than Rh black, displaying a significant dependence upon their morphologies.

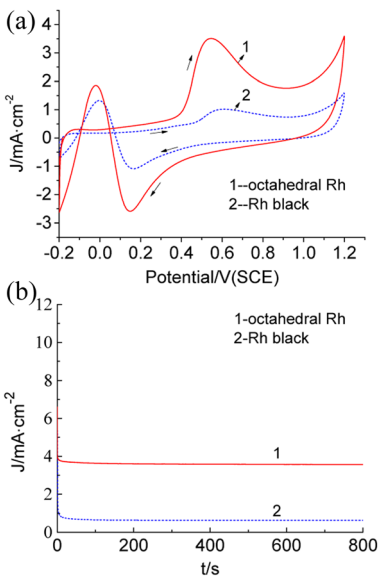

Fig. 5 The CV (a) and CA (b) curves for the electrochemical oxidation of 0.5 mol L^{-1} HCOOH over the octahedral Rh nanocrystals and Rh black in 0.5 mol L^{-1} $HClO_4$ solution, respectively.

Author contributions

X. Liu and J. Xu contributed equally to this work and should be regarded as co-first authors. All authors discussed the results and commented on the manuscript.

Conflicts of interest

There are no conflicts to declare.

Acknowledgements

This work was supported by the National Nature Science Foundation of China (Grant 21273289) and the Fundamental Research Funds for the Central Universities (CZZ20002).

Notes and references

1 C. Burda, X. Chen, R. Narayanan and M. A. El-Sayed, Chemistry and properties of nanocrystals of different shapes, *Chem. Rev.*, 2005, **105**, 1025–1102.

2 X. D. Mu, J. X. Meng, Z. C. Li and Y. Kou, Rhodium nanoparticles stabilized by ionic copolymers in ionic liquids: Long lifetime nanocluster catalysts for benzene hydrogenation, *J. Am. Chem. Soc.*, 2005, **127**, 9694–9695.

3 K. H. Park, K. Jang, H. J. Kim and S. U. Son, Near monodisperse tetrahedral rhodium nanoparticles on charcoal: The shape-dependent catalytic hydrogenation of arenes, *Angew. Chem., Int. Ed.*, 2007, **46**, 1152–1155.

4 R. R. Dykeman, N. Yan, R. Scopelliti and P. J. Dyson, Enhanced rate of arene hydrogenation with imidazolium functionalized bipyridine stabilized rhodium nanoparticle catalysts, *Inorg. Chem.*, 2011, **50**, 717–719.

5 X. Y. Quek, Y. J. Guan and E. J. M. Hensen, Structure sensitivity in the hydrogenation of unsaturated hydrocarbons over Rh nanoparticles, *Catal. Today*, 2012, **183**, 72–78.

6 Y. Jiang, J. Su, Y. Yang, Y. Jia, Q. Chen, Z. Xie and L. Zheng, A facile surfactant-free synthesis of Rh flower-like nanostructures constructed from ultrathin nanosheets and their enhanced catalytic properties, *Nano Res.*, 2016, **9**, 849–856.

7 J. Zhang, M. Chen, J. Chen, H. Li, S. Wang, Q. Kuang, Z. Cao and Z. Xie, Synthesis of single-crystal hyperbranched rhodium nanoplates with remarkable catalytic properties, *Sci. China Mater.*, 2017, **60**, 685–696.

8 B. Jiang, C. Li, O. Dag, H. Abe, T. Takei, T. Imai, M. S. A. Hossain, M. T. Islam, K. Wood, J. Henzie and Y. Yamauchi, Mesoporous metallic rhodium nanoparticles, *Nat. Commun.*, 2017, **8**, 15581.

9 C. Hou, J. Zhu, C. Liu, X. Wang, Q. Kuang and L. Zheng, Formaldehyde-assisted synthesis of ultrathin Rh nanosheets for applications in CO oxidation, *CrystEngComm*, 2013, **15**, 6127–6130.

10 Y. W. Zhang, M. E. Grass, W. Y. Huang and G. A. Somorjai, Seedless polyol synthesis and CO oxidation activity of monodisperse (111)- and (100)-oriented rhodium nanocrystals in sub-10 nm sizes, *Langmuir*, 2010, **26**, 16463–16468.

11 M. E. Grass, Y. W. Zhang, D. R. Butcher, J. Y. Park, Y. M. Li, H. Bluhm, K. M. Bratlie, T. F. Zhang and G. A. Somorjai, A reactive oxide overlayer on rhodium nanoparticles during CO oxidation and its size dependence studied by *in situ* ambient-pressure X-ray photoelectron spectroscopy, *Angew. Chem., Int. Ed.*, 2008, **47**, 8893–8896.

12 V. K. Kanuru, S. M. Humphrey, J. M. W. Kyffin, D. A. Jefferson, J. W. Burton, M. Armbruster and R. M. Lambert, Evidence for heterogeneous Sonogashira coupling of phenylacetylene and iodobenzene catalyzed by well defined rhodium nanoparticles, *Dalton Trans.*, 2009, 7602–7605.

13 S. Xie, N. Lu, Z. Xie, J. Wang, M. J. Kim and Y. Xia, Synthesis of Pd-Rh core-frame concave nanocubes and their conversion to Rh cubic nanoframes by selective etching of the Pd core, *Angew. Chem., Int. Ed.*, 2012, **51**, 10266–10270.

14 W. Ye, S. Kou, X. Guo, F. Xie, H. Sun, H. Lu and J. Yang, Controlled synthesis of bimetallic Pd-Rh nanoframes and nanoboxes with high catalytic performances, *Nanoscale*, 2015, **7**, 9558–9562.

15 R. Franke, D. Selent and A. Börner, Applied hydroformylation, *Chem. Rev.*, 2012, **112**, 5675–5732.

16 Y. Yuan, N. Yan and P. J. Dyson, Advances in the rational design of rhodium nanoparticle catalysts: Control *via* manipulation of the nanoparticle core and stabilizer, *ACS Catal.*, 2012, **2**, 1057–1069.

17 Z. Sun, Y. H. Wang, M. M. Niu, H. Q. Yi, J. Y. Jiang and Z. L. Jin, Poly(ethylene glycol)-stabilized Rh nanoparticles as efficient and recyclable catalysts for hydroformylation of olefins, *Catal. Commun.*, 2012, **27**, 78–82.

18 C. Hou, G. F. Zhao, Y. J. Ji, Z. Q. Niu, D. S. Wang and Y. D. Li, Hydroformylation of alkenes over rhodium supported on the metal–organic framework ZIF-8, *Nano Res.*, 2014, **7**, 1364–1369.

19 S. Xie, X. Y. Liu and Y. Xia, Shape-controlled syntheses of rhodium nanocrystals for the enhancement of their catalytic properties, *Nano Res.*, 2015, **8**, 82–96.

20 Y. Kang, F. Li, S. Li, P. Jin, J. Zeng, J. Jiang and Y. Chen, Unexpected catalytic activity of rhodium nanodendrites with nanosheet subunits for methanol electrooxidation in an alkaline medium, *Nano Res.*, 2016, **9**, 3893–3902.

21 N. F. Yu, N. Tian, Z. Y. Zhou, L. Huang, J. Xiao, Y. H. Wen and S. G. Sun, Electrochemical synthesis of tetrahexahedral rhodium nanocrystals with extraordinarily high surface energy and high electrocatalytic activity, *Angew. Chem., Int. Ed.*, 2014, **53**, 5097–5101.

22 J. Du, X. Wang, C. Li, X.-Y. Liu, L. Gu and H.-P. Liang, Hollow Rh nanoparticles with nanoporous shell as efficient electrocatalyst for hydrogen evolution reaction, *Electrochim. Acta*, 2018, **282**, 853–859.

23 J. Bai, G.-R. Xu, S.-H. i Xing, J.-H. Zeng, J.-X. Jiang and Y. Chen, Hydrothermal synthesis and catalytic application of ultrathin rhodium nanosheet nanoassemblies, *ACS Appl. Mater. Interfaces*, 2016, **8**, 33635–33641.

24 H.-M. Liu, S.-H. Han, Y. Zhao, Y.-Y. Zhu, X.-L. Tian, J.-H. Zeng, J.-X. Jiang, B. Y. Xia and Y. Chen, Surfactant-free atomically ultrathin rhodium nanosheet nanoassemblies for efficient nitrogen electroreduction, *J. Mater. Chem. A*, 2018, **6**, 3211–3217.

25 L. Zhao, C. Xu, H. Su, J. Liang, S. Lin, L. Gu, X. Wang, M. Chen and N. Zheng, Single-crystalline rhodium nanosheets with atomic thickness, *Adv. Sci.*, 2015, **2**, 1500–1505.

26 K. Jang, H. J. Kim and S. U. Son, Low-Temperature synthesis of ultrathin rhodium nanoplates *via* molecular orbital

symmetry interaction between rhodium precursors, *Chem. Adv. Mater.*, 2011, **22**, 1273–1275.

27 H. Duan, N. Yan, R. Yu, C.-R. Chang, G. Zhou, H.-S. Hu, H. Rong, Z. Niu, J. Mao, H. Asakura, T. Tanaka, P. J. Dyson, J. Li and Y. Li, Ultrathin rhodium nanosheets, *Nat. Commun.*, 2014, **5**, 3093–3100.

28 Y. Zhang, M. E. Grass, J. N. Kuhn, F. Tao, S. E. Habas, W. Huang, P. Yang and G. A. Somorjai, Highly selective synthesis of catalytically active monodisperse rhodium nanocubes, *J. Am. Chem. Soc.*, 2008, **130**, 5868–5869.

29 S. Yao, Y. Yuan, C. Xiao, W. Z. Li, Y. Kou, P. J. Dyson and N. Yan, Insights into the formation mechanism of rhodium nanocubes, *J. Phys. Chem. C*, 2012, **116**, 15076–15086.

30 Y. Chen, Q. S. Chen, S. Y. Peng, Z. Q. Wang, G. Lu and G. C. Guo, Manipulating the concavity of rhodium nanocubes enclosed by high-index facets *via* site-selective etching, *Chem. Commun.*, 2014, **50**, 1662–1664.

31 S. Xie, H. Zhang, N. Lu, M. Jin, J. Wang, M. J. Kim, Z. Xie and Y. Xia, Synthesis of rhodium concave tetrahedrons by collectively manipulating the reduction kinetics, facet-selective capping, and surface diffusion, *Nano Lett.*, 2013, **13**, 6262–6268.

32 S. Choi, S. R. Lee, C. Ma, B. Oliy, M. Luo, M. Chi and Y. Xia, Facile synthesis of rhodium icosahedra with controlled sizes up to 12 nm, *ChemNanoMat*, 2016, **2**, 61–66.

33 H. Zhang, W. Li, M. Jin, J. Zeng, T. Yu, D. Yang and Y. Xia, Controlling the morphology of rhodium nanocrystals by manipulating the growth kinetics with a syringe pump, *Nano Lett.*, 2011, **11**, 898–903.

34 J. D. Hoefelmeyer, K. Niesz, G. A. Somorja and T. D. Tilley, Radial Anisotropic Growth of Rhodium Nanoparticles, *Nano Lett.*, 2005, **5**, 435–438.

35 N. Zettsu, J. M. McLellan, B. Wiley, Y. Yin, Z. Y. Li and Y. Xia, Synthesis, stability, and surface plasmonic properties of rhodium multipods, and their use as substrates for surface-enhanced raman scattering, *Angew. Chem., Int. Ed.*, 2006, **45**, 1288–1292.

36 S. M. Humphrey, M. E. Grass, S. E. Habas, K. Niesz, G. A. Somorjai and T. D. Tilley, Rhodium Nanoparticles from Cluster Seeds: Control of Size and Shape by Precursor Addition Rate, *Nano Lett.*, 2007, **7**, 785–790.

37 K. W. Lee, J. Park, H. Lee, D. Yoon, H. Baik, S. Haam, J.-H. Sohn and K. Lee, Morphological evolution of 2D Rh nanoplates to 3D Rh concave nanotents, hierarchically stacked nanoframes, and hierarchical dendrites, *Nanoscale*, 2015, **7**, 3460–3465.

38 H. Kim, N. T. Khi, J. Yoon, H. Yang, Y. Chae, H. Baik, H. Lee, J. H. Sohn and K. Lee, Fabrication of hierarchical Rh nanostructures by understanding the growth kinetics of facet-controlled Rh nanocrystals, *Chem. Commun.*, 2013, **49**, 2225–2227.

39 J. Zhang, J. Ye, Q. Fan, Y. Jiang, Y. Zhu, H. Li, Z. Cao, Q. Kuang, J. Cheng and J. Zheng, Cyclic penta-twinned rhodium nanobranches as superior catalysts for ethanol electro-oxidation, *J. Am. Chem. Soc.*, 2018, **140**, 11232–11240.

40 H. Zhang, X. Xia, W. Li, J. Zeng, Y. Dai, D. Yang and Y. Xia, Facile Synthesis of Five-fold Twinned, Starfish-like Rhodium Nanocrystals by Eliminating Oxidative Etching with a Chloride-free Precursor, *Angew. Chem., Int. Ed.*, 2010, **49**, 5296–5300.

41 J. Park, J. Kim, Y. Yang, D. Yoon, H. Baik, S. Haam, H. Yang and K. Lee, RhCu 3D nanoframe as a highly active electrocatalyst for oxygen evolution reaction under alkaline condition, *Adv. Sci.*, 2016, **3**, 1500252.

42 W. Fu, Y. Lu, Y. Fang, M. Su, Y. Zhao and T. Huang, Highly symmetrical Rh nanonail flowers, *ChemNanoMat*, 2020, **6**, 1870–1875.

43 J. F. Moulder, W. F. Stickle, P. E. Sobol and K. D. Bomben, in *Handbook of X-ray Photoelectron Spectroscopy*, Perkin-Elmer Co., Eden Prairie, M. N., 1992.

44 J. Xu, H. Tang, B. Ning, Y. Zhao and T. Huang, Microwave-assisted synthesis of mutually embedded Rh concave nanocubes with enhanced electrocatalytic activity, *RSC Adv.*, 2019, **9**, 19126–19130.

45 J. Yang, M. Su, Y. Zhao, J. Li, M. Li and T. Huang, Facile Microwave-assisted synthesis of concave octahedral Pt-Cu alloy nanocrystals and their electrocatalytic properties, *ChemNanoMat*, 2018, **4**, 909–913.

46 L. Dai, Y. Zhao, Q. Chi, H. Liu, J. Li and T. Huang, Morphological control and evolution of octahedral and truncated trisoctahedral Pt-Au alloy nanocrystals under microwave irradiation, *Nanoscale*, 2014, **6**, 9944–9950.

47 L. Dai, Q. Chi, Y. Zhao, H. Liu, Z. Zhou, J. Li and T. Huang, Controlled synthesis of novel octapod platinum nanocrystals under microwave irradiation, *Mater. Res. Bull.*, 2014, **49**, 413–419.

48 S. E. Lohse, N. D. Burrows, L. Scarabelli, L. M. Liz-Marzán and C. J. Murphy, Anisotropic noble metal nanocrystal growth: the role of halides, *Chem. Mater.*, 2014, **26**, 34–43.

49 B. T. Sneed, M. C. Golden, Y. Liu, H. K. Lee, I. Andoni, A. P. Young, G. McMahon, N. Erdman, M. Shibata, X. Y. Ling and C.-K. Tsung, Promotion of the halide effect in the formation of shaped metal nanocrystals *via* a hybrid cationic, polymeric stabilizer: octahedra, cubes, and anisotropic growth, *Surf. Sci.*, 2016, **648**, 307–312.

50 G. Chen, C. Xu, X. Huang, J. Ye, L. Gu, G. Li, Z. Tang, B. Wu, H. Yang, Z. Zhao, Z. Zhou, G. Fu and N. Zheng, Interfacial electronic effects control the reaction selectivity of platinum catalysts, *Nat. Mater.*, 2016, **15**, 564–569.